

Role of the van Hove Singularity in the Quantum Criticality of the Hubbard Model

K.-S. Chen*, S. Pathak*, S.-X. Yang*, S.-Q. Su†, D. Galanakis**, K. Mikelson‡, M. Jarrell* and J. Moreno*

**Department of Physics and Astronomy, Louisiana State University, Baton Rouge, LA 70803, USA*

†*Oak Ridge National Laboratory, Oak Ridge, Tennessee 37831, USA*

***Nanyang Technological University, Singapore 639798*

‡*Department of Physics, Georgetown University, Washington DC, 20057, USA*

(Dated: June 2, 2019)

A quantum critical point (QCP), separating the non-Fermi liquid region from the Fermi liquid, exists in the phase diagram of the two-dimensional Hubbard model [Vidhyadhiraja *et. al*, Phys. Rev. Lett. **102**, 206407 (2009)]. Due to the vanishing of the critical temperature associated with a phase separation transition, the quantum critical point is characterized by a vanishing quasiparticle weight. Near the quantum critical point, the pairing is enhanced since the real part of the bare d -wave particle-particle susceptibility exhibits algebraic divergence with decreasing temperature, replacing the logarithmic divergence found in a Fermi liquid [Yang *et. al*, Phys. Rev. Lett. **106**, 047004 (2010)]. In this paper we explore the van Hove singularity in the dispersion crossing the Fermi level near the quantum critical filling and examine its role in determining the critical algebraic behavior of the bare susceptibility. We calculate the bare susceptibility to a d -wave pair field for the usual two-dimensional tight binding dispersion and a hypothetical quartic dispersion. We find that the usual logarithmic van Hove singularity cannot correctly describe the critical algebraic behavior and it is essential to have an extended van Hove singularity that has an algebraic singularity in the density of states. The extended van Hove singularity is found to be pinned near the Fermi level for a larger range of doping on the inclusion of a next-near-neighbor hopping $t' < 0$. Transport properties near the quantum critical point are investigated using high quality estimates of the self energy obtained by *direct* analytic continuation of self energy from Continuous-Time Quantum Monte Carlo. Resistivity, thermal conductivity, Wiedemann-Franz Law, and thermopower are examined in the Fermi liquid, Marginal Fermi liquid, and pseudo-gap regions. A next-near-neighbor hopping $t' < 0$ increases the doping region where the marginal Fermi liquid character is found, consistent with the van Hove singularity picture. Both T and negative t' are relevant variables for the quantum critical point, and both the transport and the motion of the van Hove singularity with filling suggest that they are roughly isotropic in their effect.

I. INTRODUCTION

A plausible scenario for the high temperature superconductivity in cuprates is based upon the presence of a van Hove singularity corresponding to the saddle points in the single particle energy dispersion.¹⁻⁴ These flat regions in the energy dispersion are directly observed in ARPES experiments on various cuprate compounds.⁵⁻⁹ Recently, it was also observed in the tunneling spectra of Bi-2201.¹⁰ If the Fermi level is made to coincide with the van Hove singularity by means of doping, then the superconducting transition temperature is greatly enhanced. The van Hove scenario is also argued¹¹⁻¹³ to be responsible for the “*marginal Fermi liquid*” behavior¹⁴ in which the lifetime broadening of the quasiparticles is of the order of its frequency. Thus the van Hove scenario can account for the linear- T resistivity,^{12,13,15} T -independent thermopower,¹² anomalous isotope effect¹³ etc.

There is numerical evidence for van Hove singularity in strongly correlated systems. The energy dispersion of one hole in an antiferromagnetic background has been considered in theoretical studies on the Hubbard model^{16,17} and t - J model.¹⁸ These studies report the presence of extended saddle points. Assaad and Imada¹⁶ found that the dispersion has a quartic form \mathbf{k}^4 near the anti-nodal point $(\pi, 0)$. A recent account of the presence of an extended saddle point in energy dispersion due to the elec-

tronic correlations found in graphene argued that it leads to a superconducting instability.¹⁹

These examples of extended saddle points in various correlated superconducting systems and their proximity to the Fermi level at the doping where the maximum T_c occurs, demonstrate that it is extremely important to understand the role played by these singularities. A plethora of scientific efforts have been devoted towards achieving this understanding.²⁰⁻³⁴ At the simplest level, the role of the van Hove singularity may be interpreted within the BCS formalism. Here, the condition for T_c is when the strength of the pairing interaction times the real part of the bare pairing polarization $V\chi'_0(\omega = 0) = 1$. In a BCS superconductor, $\chi'_0(\omega = 0)$ displays a logarithmic divergence as $T \rightarrow 0$, yielding the BCS exponential form for T_c . The van Hove singularity enhances the divergence of $\chi'_0(\omega = 0)$, replacing the logarithm by a stronger function of T , yielding higher transition temperatures.

However, there is also strong evidence for the proximity of the maximum T_c and a quantum critical point (QCP) located beneath the superconducting dome in the cuprates.^{35,36} Above the QCP, the in-plane resistivity is known to vary linearly with T over a wide range of temperatures yet narrow range of doping which characterizes the marginal Fermi liquid behavior.³⁷⁻⁴³ The resistivity increases as the doping decreases from the Fermi Liquid into the pseudogap region. Especially in the Fermi liq-

uid region, the low temperature resistivity varies as T^2 , characteristic of a Fermi liquid. Moreover, the thermal conductivity (κ),^{44,45} thermopower (S)^{46,47} and tunneling conductance (g)⁴⁸ have been investigated near the QCP of cuprates. κ is observed to be nearly independent of temperature in the marginal Fermi liquid state⁴⁹ and depends on $1/T$ in the Fermi liquid consistent with the Wiedemann-Franz Law,⁵⁰ $\kappa\rho \propto T$. Chakraborty et al.⁵¹ suggested that the thermopower changes sign abruptly near the optimal doping in most of the cuprate materials, corresponding to a state in which the particle-hole symmetry is generated. Also in the marginal Fermi liquid, the tunneling conductance $g(V) \sim g_0 + g_1|V|$, where g_0 and g_1 weakly depend on T and V is up to 0.1eV. To explain the anomalous transport properties of the marginal Fermi liquid, Varma et al.^{14,52} proposed an analytical form of the single-particle self energy in the marginal Fermi liquid.

A recent study⁵³ reported the presence of a quantum critical point in the two-dimensional Hubbard model that separates the non-Fermi liquid pseudogap region from the Fermi liquid region. At finite temperatures, the two phases are separated by the marginal Fermi liquid. At this QCP, the quasiparticle spectral weight Z becomes zero. Interestingly, at the QCP, the density of states (DOS) is found to be nearly particle-hole symmetric at low frequencies with a sharp peak at $\omega = 0$. This filling is tantalizingly close to the optimal doping where the superconducting transition temperature T_c attains its maximum. This naturally raises the question about the role played by the van Hove singularity in the quantum criticality and its possible connection to the large superconducting T_c .

The proximity of the superconducting dome to the QCP in the two-dimensional Hubbard model was recently investigated by Yang et al.⁵⁴ in a Dynamical Cluster Approximation (DCA) study of the bare d-wave pairing susceptibility (χ_{0d}). Unlike the BCS case, where the real part of the bare susceptibility displays a logarithmic divergence as $T \rightarrow 0$ leading to the BCS exponential equation for T_c , Yang et al.⁵⁴ found that $\chi'_{0d}(\omega = 0)$ decays algebraically as $\frac{1}{\sqrt{T}}$ at the QCP, thus leading to a strongly enhanced dressed pairing susceptibility and T_c . The real part of the susceptibility is related to the imaginary part of the susceptibility through the Kramers-Krönig relation: $\chi'(T) = \frac{1}{\pi} \int \frac{\chi''(\omega)}{\omega} d\omega$. The algebraic divergence of the real part of the susceptibility $\chi'(T)$ was found to come from a scaling behavior of the imaginary part $\chi''(\omega)$ - when $T^{3/2}\chi''(\omega)/\omega$ is plotted against ω/T , the different temperature curves fall on each other determined by a scaling function $H(x)$ defined by $T^{3/2}\chi''(\omega)/\omega = H(\omega/T) \approx (\omega/T)^{-3/2}$ (see Fig. 1). The contribution from H to $\chi'(T) = \frac{T^{-3/2}}{\pi} \int H(\omega/T) d\omega \propto T^{-1/2}$ which will dominate at low T . As shown in the inset, $\chi''(\omega)/\omega|_{\omega=0}$ rises linearly with $1/T$ as expected for a Fermi liquid, when $n = 0.75$. For lower doping, $\chi''(\omega)/\omega|_{\omega=0}$ rises more slowly, so that at the quantum

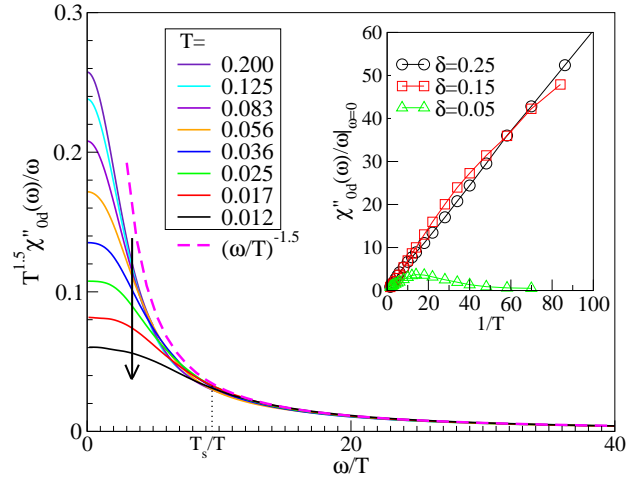


FIG. 1: (color online) Frequency dependence of the imaginary part of the particle-particle d -wave susceptibility obtained from the DCA method for various temperatures at the critical filling $n = 0.85$. All the curves fall on top of each other for frequencies greater than $\omega/T \approx J/4t$. (Taken from Yang et al.⁵⁴)

critical doping, $H(0) = 0$, indicating that there is no contribution to H coming from particles at the Fermi energy.

In this manuscript, we use the Dynamical Cluster Quantum Monte Carlo method to explore the relationship between the QCP and van Hove singularity scenarios for high-temperature superconductivity in the Hubbard model. We successfully obtain high quality estimates of the real-frequency single-particle self energy $\Sigma(\mathbf{K}, \omega)$ by direct analytic continuation of the Matsubara self energy $\Sigma(\mathbf{K}, i\omega_n)$ using the Maximum Entropy Method.^{55,56} The self energy does not have artifacts that come about by inverting the coarse-grained Dyson's equation.⁵⁵ We summarize this method in section II. In the model with next-near-neighbor hopping $t' = 0$, we find that as we dope the system across the quantum critical filling, an extended flat region in the dispersion passes through the Fermi level E_F , accompanied by a sharp nearly symmetric peak in the DOS which also passes quickly through the Fermi level. We find that the resistivity in Fig. 14 has a linear- T property over a wide range of temperatures yet a narrow range of doping. We use these high quality estimates of the self energy to calculate the bare pairing polarization, we again find the collapse of the data found in Fig. 1. To understand the role played by the van Hove singularity in determining this critical behavior, we have calculated the particle-particle susceptibility in the d -channel for two models at half filling - standard quadratic dispersion and a hypothetical quartic dispersion. While these forms can yield the observed algebraic divergence of $\chi'_{0d}(\omega = 0)$, they do not yield the collapse of data found in Fig. 1, suggesting that a van Hove singularity alone does not capture the phenomena. When t' becomes negative, the system deviates from the QCP and

the resistivity in Fig. 14 has the linear- T property over a wider range of doping, and the sharp peak in the DOS and the flat region of the dispersion linger near the Fermi level for a wider range of doping. These results suggest that the doping region of low temperature quantum criticality becomes larger when $t' < 0$. We also show that the zero-frequency self energy $\text{Im}\Sigma(T, \omega = 0)$, the dominant contribution to the resistivity, has a wider range of linear- T behavior for $t' < 0$ than $t' = 0$, and this embodies the phase diagram near the QCP. We will discuss the phase diagram in section IV.

This paper has been organized as follows: Section II briefly outlines the model and methods used in this study. Results are presented in section III. The susceptibility calculation is discussed in section III B, effect of t' on dispersion in III C and transport results in III D. The paper is concluded with the discussion in section IV.

II. FORMALISM

In this work, we look for direct evidence of the van Hove singularity and the marginal Fermi liquid behavior in the spectra, electronic dispersion, and transport properties of the two-dimensional Hubbard model

$$H = H_k + H_p = \sum_{\mathbf{k}\sigma} \epsilon_{\mathbf{k}}^0 c_{\mathbf{k}\sigma}^\dagger c_{\mathbf{k}\sigma} + U \sum_i n_{i\uparrow} n_{i\downarrow}, \quad (1)$$

where $c_{\mathbf{k}\sigma}^\dagger$ ($c_{\mathbf{k}\sigma}$) is the creation (annihilation) operator for electrons with wavevector \mathbf{k} and spin σ , $n_{i\sigma} = c_{i\sigma}^\dagger c_{i\sigma}$ is the number operator, and the bare dispersion is

$$\epsilon_{\mathbf{k}}^0 = -2t(\cos k_x + \cos k_y) - 4t'(\cos k_x \cos k_y - 1) \quad (2)$$

with t and t' being the hopping amplitude between the nearest-neighbor sites and the next-near-neighbor sites respectively. U is the on-site Coulomb repulsion.

We employ the Dynamical Cluster Approximation (DCA)^{57,58} to study this model with a Quantum Monte Carlo (QMC) algorithm as the cluster solver. The DCA is a cluster mean-field theory that maps the original lattice onto a periodic cluster of size $N_c = L_c^2$ embedded in a self-consistently determined host. This many-to-one map is accomplished by dividing the lattice Brillouin zone into cells centered at momenta \mathbf{K} , and coarse graining the lattice Green's functions by summing over the momenta labeled with $\tilde{\mathbf{k}}$ within each cell

$$\bar{G}(\mathbf{K}, \omega) = \frac{N_c}{N} \sum_{\tilde{\mathbf{k}}} G(\mathbf{K} + \tilde{\mathbf{k}}, \omega), \quad (3)$$

where \bar{G} and G are the coarse-grained and the lattice single-particle propagators respectively. The coarse-grained Green's function defines the cluster problem. Spatial correlations up to a range L_c within the cluster are treated explicitly, while those at longer length scales are described at the mean-field level. However the

correlations in time, essential for quantum criticality, are treated explicitly for all cluster sizes. To solve the cluster problem, we use the Hirsch-Fye QMC method^{59,60} (only for the charge susceptibility in Fig. 2) and the Continuous-Time QMC⁶¹ which has no Trotter error.⁶² We employ the Maximum Entropy Method⁵⁵ to calculate the real-frequency spectra.

A. Calculation of Single-Particle Spectra

In previous calculations of the single-particle spectra, we analytically continue the QMC $\bar{G}(\mathbf{K}, \tau)$ to obtain $\bar{G}(\mathbf{K}, \omega)$, and then invert the coarse-graining Eqn. (3) for the self energy $\Sigma(\mathbf{K}, \omega)$. This last step can introduce spurious features in $\Sigma(\mathbf{K}, \omega)$. As observed previously,⁵⁶ it is better to analytically continue the self energy directly. However, the self energy spectra does not share the normalization of $\int d\omega \bar{A}(\mathbf{K}, \omega) = 1$, where $\bar{A}(\mathbf{K}, \omega) = \frac{-1}{\pi} \text{Im}\bar{G}(\mathbf{K}, \omega)$. This normalization is a desirable feature since it allows us to treat the spectrum as a normalized probability distribution. Since the Hubbard $\Sigma(\mathbf{K}, \omega_n) = \Sigma_H + U^2 \chi_{\sigma,\sigma} / i\omega_n + \dots$, where $\chi_{\sigma,\sigma} = \langle n_\sigma n_\sigma \rangle - \langle n_\sigma \rangle^2 = n_\sigma(1 - n_\sigma)$ is the local polarizability of a single spin species σ and $\Sigma(\mathbf{K}, \omega_n) - \Sigma_H = \int d\omega (-\frac{1}{\pi}) \Sigma(\mathbf{K}, \omega) / (i\omega_n - \omega)$. It is easy to see that the integral of $\Sigma(\mathbf{K}, \omega_n) - \Sigma_H$ is $U^2 \chi_{\sigma,\sigma}$. Therefore we will analytically continue

$$\frac{\Sigma(\mathbf{K}, \omega_n) - \Sigma_H}{U^2 \chi_{\sigma,\sigma}} = \int d\omega \frac{\sigma(\mathbf{K}, \omega)}{i\omega_n - \omega}, \quad (4)$$

where $\sigma(\mathbf{K}, \omega) = -\frac{1}{\pi} \Sigma(\mathbf{K}, \omega) / U^2 \chi_{\sigma,\sigma}$, $\int d\omega \sigma(\mathbf{K}, \omega) = 1$, using $\chi_{\sigma,\sigma}$ calculated in the QMC process. Then we obtain the lattice self energy $\Sigma(\mathbf{k}, \omega)$ by interpolating the cluster self energy $\Sigma(\mathbf{K}, \omega)$ to get the single-particle spectral function $A(\mathbf{k}, \omega)$.

B. Susceptibility to the d -wave Pair Field

We calculate the susceptibility in the d -wave channel to the pair field $\mathcal{V} = -f_d b_d^\dagger + \text{h.c}$ for various models having a van Hove singularity at the Fermi level. Here $b_d^\dagger = \frac{1}{2} \sum_i (b_{i+\hat{x}}^\dagger - b_{i+\hat{y}}^\dagger)$ is the singlet creation operator, where $b_{i+\hat{\alpha}}^\dagger$ creates a singlet at bond $i-(i+\hat{\alpha})$, ($\alpha = x, y$) and f_d is a complex constant. The susceptibility χ'_{0d} can be computed by calculating the following bubble

$$\chi'_{0d}(T) = \frac{1}{\beta} \sum_{\mathbf{k}, i\omega_n} g_d^2(\mathbf{k}) G^0(\mathbf{k}, i\omega_n) G^0(-\mathbf{k}, -i\omega_n), \quad (5)$$

where β is the inverse temperature, $\omega_n = \frac{(2n+1)\pi}{\beta}$ are the odd Matsubara frequencies and $g_d(\mathbf{k})$ is the d -wave form factor given by

$$g_d(\mathbf{k}) = \cos k_x - \cos k_y. \quad (6)$$

$G^0(\mathbf{k}, i\omega_n)$ is the bare Green's function given by

$$G^0(\mathbf{k}, i\omega_n) = \frac{1}{i\omega_n - \epsilon_{\mathbf{k}}^0}. \quad (7)$$

$\epsilon^0(\mathbf{k})$ is the bare band dispersion in Eqn. (2). χ'_{0d} can be evaluated using the standard Matsubara summation which gives

$$\chi'_{0d}(T) = \sum_{\mathbf{k}} g_d^2(\mathbf{k}) \left(\frac{1 - 2f_{\mathbf{k}}}{2\epsilon_{\mathbf{k}}^0} \right), \quad (8)$$

where $f_{\mathbf{k}}$ is the Fermi function.

C. Details of Transport Calculations

The main hypothesis of the marginal Fermi liquid^{14,52} is that for a wide range of wavevectors \mathbf{q} , excitations exist that makes a contribution to the spin and charge susceptibilities reflected by

$$\chi''(\mathbf{q}, \omega) \propto \min(|\omega/T|, 1) \text{sign}(\omega). \quad (9)$$

Electrons scattering from these excitations acquire a self energy

$$\Sigma(\mathbf{k}, \omega) \propto \omega \ln(x/\omega_c) - i\pi x/2, \quad (10)$$

where $x = \max(|\omega|, T)$, and ω_c is a cutoff. The marginal Fermi liquid ansatz has several consequences on experimentally relevant quantities, including transport anomalies, such as the linear- T electrical resistivity, the tunneling conductance $g(V) \sim g_0 + g_1|V|$, the photoemission, the nuclear relaxation rate $T_1^{-1} \sim aT + b$, the optical conductivity $\sigma(\omega)$, the Raman scattering, and the superconductive pairing. For the specific heat $C_v(T)$ and thermal conductivity $\kappa(T)$, Varma argues that the normal state's electronic contribution is hardly extracted from the experimental data due to a large phonons' contribution. The thermal conductivity from the electronic contribution approximates to a constant because the Wiedemann-Franz law roughly holds for the marginal Fermi liquid.

We use the Kubo formula⁶³ to calculate the Onsager transport coefficients:

$$L_{\alpha\beta}^{ij} = \pi \int d\omega \left(-\frac{df}{d\omega} \right) \omega^{i+j-2} \mathcal{D}_{\alpha\beta}(\omega), \quad (11)$$

where f is the Fermi function and

$$\mathcal{D}_{\alpha\beta}(\omega) = \frac{1}{N} \sum_{\mathbf{k}} v^\alpha(\mathbf{k}) v^\beta(\mathbf{k}) A(\mathbf{k}, \omega)^2, \quad (12)$$

where $v^\alpha(\mathbf{k})$ is the α -component of the electron group velocity and A is the single-particle spectral function obtained in section II A. The different transport coefficients are given by the combinations of L^{ij} . For example, in units where $e = 1$ and the chemical potential $\mu = 0$, the resistivity $\rho(T) = 1/L^{11}$, the thermopower $S = -L^{12}/(TL^{11})$, the thermal conductivity

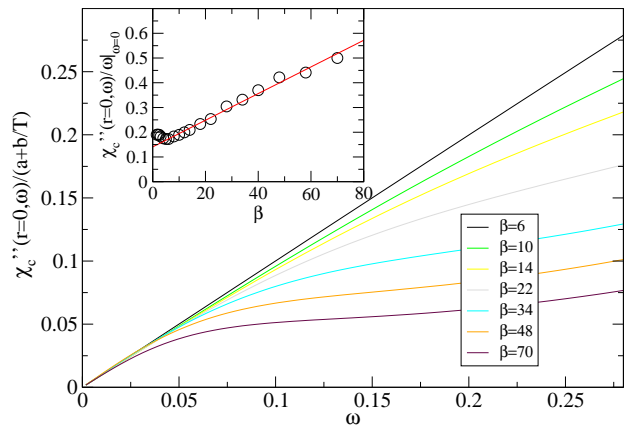


FIG. 2: (Color online) The local $\mathbf{r} = 0$ dynamic charge susceptibility divided by the initial slope when $U = 6t$, $4t = 1$, $N_c = 16$ and $t' = 0$, and it satisfies the marginal Fermi susceptibility in Eqn. (9).

$\kappa = \frac{1}{T} (L^{22} - (L^{12})^2/L^{11})$, and the Peltier coefficient $\Pi = L^{21}/L^{11}$.

We note that a simpler estimate exists for the thermopower S . Here, we perform a Sommerfeld expansion of L^{12} at the Fermi level ($\omega = 0$) and get an alternative form:

$$S = -\frac{\pi^2}{3} T \log[\mathcal{D}_{\alpha\beta}(\omega)]|_{\omega=0}. \quad (13)$$

If the electron group velocity is a constant, and the square of the single-particle spectra can be approximated by $\delta(\omega)\tau$, where τ is the relaxation time and is also assumed as a constant, the thermopower over temperature is just the derivative of the logarithm of the DOS at the Fermi level.⁶⁴

III. RESULTS

A. Single Particle Properties for $t' = 0$

We first explore the charge polarizability. The local charge polarizability $\chi_c''(\mathbf{r} = 0, \omega)$ is plotted in Fig. 2. The main plot shows $\chi_c''(\mathbf{r} = 0, \omega)$ divided by this initial slope so that the curves coincide for low ω . At higher frequencies, the curves break from this linear rise at a frequency roughly proportional to the temperature. The inset shows that the zero frequency slope of $\chi_c''(\mathbf{r} = 0, \omega)/\omega|_{\omega=0}$ is roughly linear in inverse temperature, as expected for the marginal Fermi liquid susceptibility in Eqn. (9), up to $T \approx 0.2$ or roughly $2J$. The spin polarization (not shown) does not show such an extended region of the marginal Fermi liquid character.

Fig. 3 shows the Fermi liquid ($n = 0.75$), marginal Fermi liquid ($n = 0.85$) and pseudo-gap ($n = 0.95$) self energies as a function of frequency along the anti-nodal

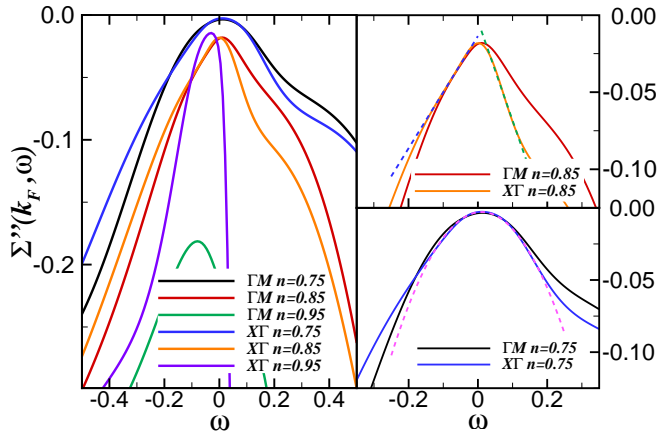


FIG. 3: (Color online) Frequency dependence of the imaginary part of the self energy $\Sigma''(\mathbf{k}_F, \omega)$ along ΓM and $X\Gamma$ when $U = 6t$, $N_c = 16$, $4t = 1$, and $t' = 0$. Dashed lines fit linearly for $n = 0.85$ and quadratically for $n = 0.75$.

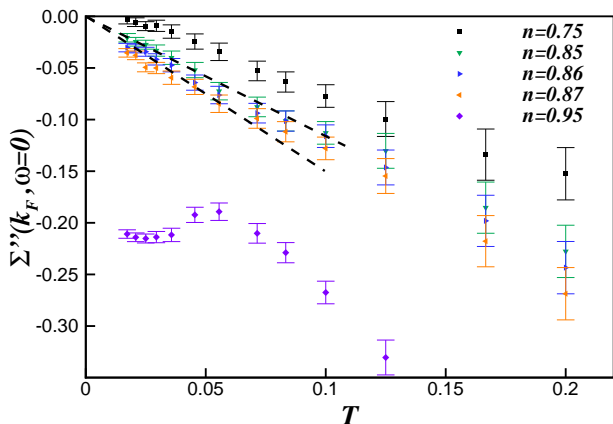


FIG. 4: (Color online) Temperature dependence of the imaginary part of the self energy $\Sigma''(\mathbf{k}_F, \omega = 0)$ when $U = 6t$, $N_c = 16$, $4t = 1$, and $t' = 0$. The linear dashed lines fit the self energies for $n = 0.85$ and 0.86 to show linear- T behavior.

($X\Gamma$) and the nodal (ΓM) directions. For the Fermi liquid self energy, the quadratic dashed line provides good fit to $\Sigma''(\mathbf{k}_F, \omega)$ for small ω as expected for the Fermi liquid theory.⁶⁵ The marginal Fermi liquid self energy has a form given by Eqn. (10), which states that the self energy is proportional to negative temperature when frequency is small and proportional to negative ω when temperature is small. The marginal Fermi liquid self energy in Fig. 3 shows linear behavior but interestingly with *different* slopes for positive and negative ω , which is unexpected considering Eqn. (10). Fig. 4 shows the temperature dependence of the self energy when $\omega = 0$ and $t' = 0$. Again we get a result consistent to Eqn. (10): $\Sigma''(\mathbf{k}_F, \omega \rightarrow 0) \propto -T$ around the marginal Fermi liquid

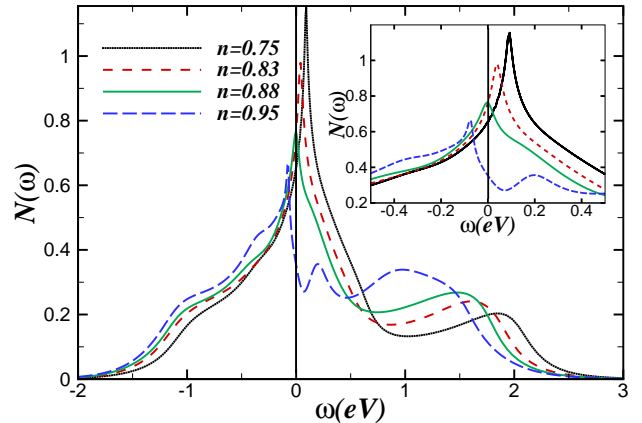


FIG. 5: (Color online) The single-particle density of states when $t' = 0$, $U = 6t$, $N_c = 16$, $4t = 1$, and $\beta = 58$. The DOS shows low-energy particle-hole symmetry at the filling $n = 0.88$.

filling for $n = 0.85$ and 0.86 . The dashed lines are linear fits. The error bars are estimated by changing different random seeds in the QMC data.

The density of states from the Fermi liquid to the pseudo-gap fillings are shown in Fig. 5. Since we have highly enhanced the quality of the self energy by *direct* analytic continuation of $\Sigma(K, i\omega_n)$, the DOS in Fig. 5 shows sharper features as compared to the results of Vidhyadhiraja et al.⁵³ As the doping decreases from the Fermi liquid to the pseudo-gap regions, the peak of DOS moves from positive energy to negative energy while its intensity is reduced. For $n = 0.95$, a pseudogap begins to open and a peak begins to form at positive frequencies. The half-filled case ($n = 1$, not shown) shows upper and lower Hubbard bands located at positive and negative ω , respectively. The DOS for filling 0.88 shows a low-frequency particle-hole symmetry, close to the critical filling 0.85 .

Fig. 6 shows the dispersion obtained from the peaks of the spectral function $A(\mathbf{k}, \omega)$ obtained using the DCA method for four fillings: $n = 0.85$, $n = 0.87$, $n = 0.88$ and $n = 0.95$ around the Fermi vector k_F along the anti-nodal direction. For a particular filling, the left panel shows the dispersion along k_x direction around k_F while the right panel shows the dispersion along k_y direction. A common identifiable feature for all fillings is the presence of an extended flat region in the dispersion. This flat region is responsible for the van Hove singularity in the density of states. Interestingly, the van Hove singularity passes through the Fermi level at a filling of $n \approx 0.88$, which is near the quantum critical filling where the quasi-particle weight Z goes to zero along the anti-nodal direction.

It is very interesting to note that the dispersion around the singularity is not quadratic as should be the case for the bare dispersion but is more “flat”. It is so flat that it looks extended in nature and it is not possible

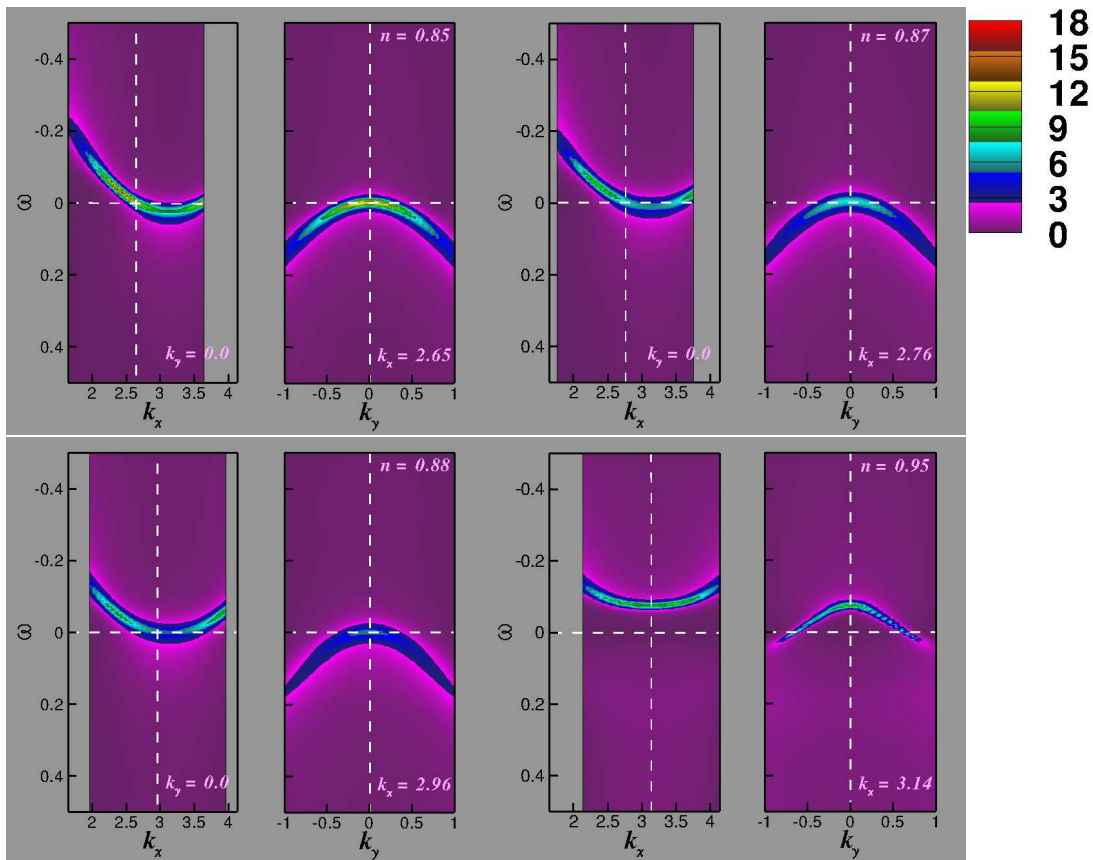


FIG. 6: (color online) Energy dispersion obtained from the peaks of the spectral function $A(\mathbf{k}, \omega)$ for various fillings around the Fermi vector k_F along the anti-nodal direction for $t' = 0$.

to fit a simple quadratic or quartic analytical form to the dispersion around $(\pi, 0)$. This can be clearly seen in Fig. 7 by the broad flat region in the dispersion along the k_x direction around the Fermi vector k_F along the anti-nodal direction for various fillings. We will see that this will have implications for the critical behavior of the particle-particle susceptibility in section III B.

B. Bare and dressed Susceptibility for $t' = 0$

Here we calculate the susceptibility in the d -wave channel for the most simple model having a van Hove singularity at the Fermi level, i.e., the tight binding model at half filling. The DOS for the dispersion given by eqn. 2 has a logarithmic singularity at $\epsilon = 0$ with the form:

$$N(\epsilon) = \log |\epsilon|. \quad (14)$$

Eqn. (8) can be converted to an integral over ω cutoff by temperature T and this will give the temperature dependence of χ'_{0d} to be $-(\log T)^2$. This is confirmed by explicit calculation of the sum in Eqn. (8) as illustrated in Fig. 8. As shown in the inset, the imaginary part does not show scaling behavior as seen in Fig. 1.

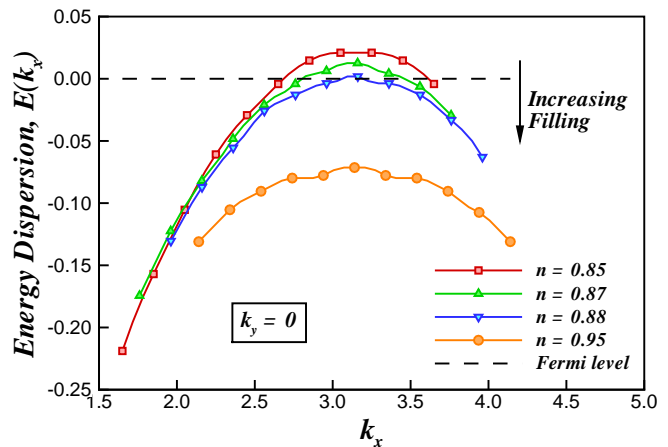


FIG. 7: (color online) Single particle dispersion around the Fermi vector k_F taken along the anti-nodal direction.

Clearly this simplistic model doesn't incorporate the strong correlation effects which strongly modify the single particle energy dispersion near $(\pi, 0)$. This makes the dispersion more flat. Drawing motivation by the “flatter”

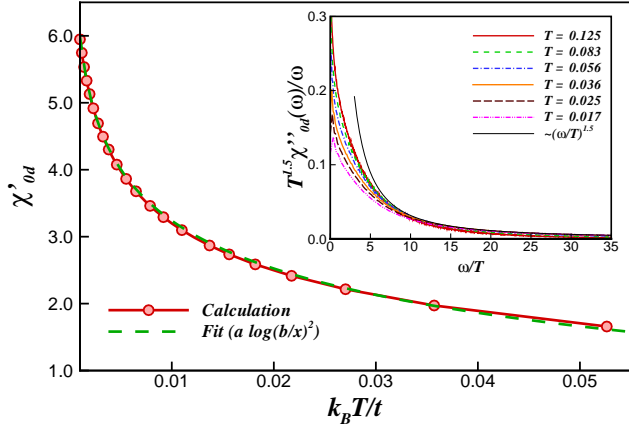


FIG. 8: (color online) (main) Temperature dependence of the real part of the particle-particle d -wave susceptibility at $\omega = 0$ for the two-dimensional bare dispersion at half filling. Note that χ'_{0d} decays logarithmically. (inset) Frequency dependence of the imaginary part of the particle-particle d -wave susceptibility for various temperatures for the two-dimensional bare dispersion at half filling. Note that the curves corresponding to various temperatures do not scale at large frequencies.

nature of the dispersion around the Fermi vector in Fig. 6 and Fig. 7, we consider the next higher order model than the quadratic dispersion allowed by the symmetry of the square lattice, i.e., a hypothetical model with a quartic dispersion

$$\epsilon_{\mathbf{k}} = -\frac{4}{\pi^4} \left((|k_x| - \pi)^4 - k_y^4 \right). \quad (15)$$

The reason for choosing this model is not purely academic. Such an extended form has been observed in experiments⁶ and also confirmed by theoretical studies.¹⁷ The low energy density of states for the quartic dispersion can be shown to be $N(\epsilon) \sim \sqrt{|\epsilon|}$.²⁵ Following the similar logic that we used for the standard dispersion in Eqn. (2), for a quartic dispersion, we get

$$\chi'_{0d} \sim \frac{1}{\sqrt{T}}. \quad (16)$$

This explicit calculation of sum in Eqn. (8) is shown in Fig. 9 and is consistent with analytical arguments above. Though the temperature dependence of the real part of the bare susceptibility is found to be algebraic for this model having flatter singularity, the inset reveals that it does not exhibit the scaling found for the imaginary part in Yang et al.⁵⁴. Thus, the simple non-interacting picture of the van Hove singularity at Fermi level does not completely describe the true temperature dependence of the susceptibility.

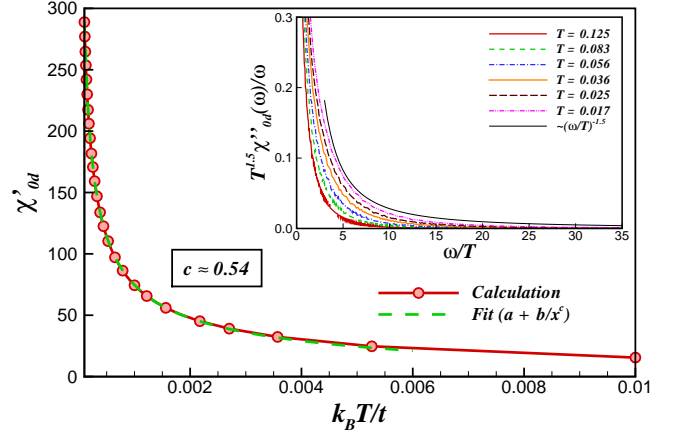


FIG. 9: (color online) (main) Temperature dependence of the real part of the particle-particle d -wave susceptibility at $\omega = 0$ for the quartic dispersion at half filling. Note that χ'_{0d} decays algebraically as $1/\sqrt{T}$. (inset) Frequency dependence of the imaginary part of the particle-particle d -wave susceptibility for various temperatures for the quartic dispersion at half filling. Note that the curves corresponding to various temperatures does not scale well at large frequencies.

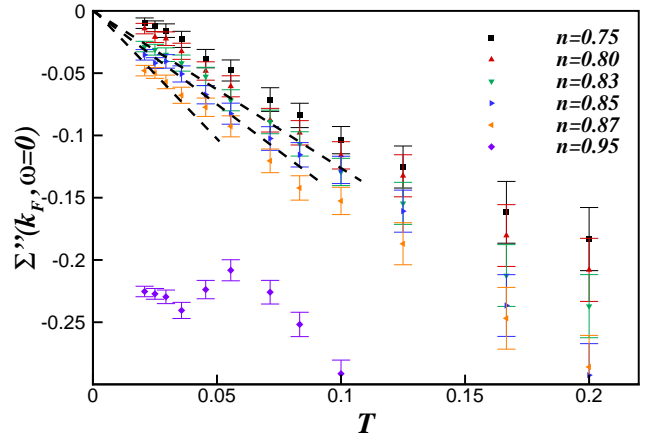


FIG. 10: (Color online) Temperature dependence of the imaginary part of the self energy $\Sigma''(\mathbf{k}_F, \omega = 0)$ when $U = 6t$, $N_c = 16$, $4t = 1$, and $t'/t = -0.1$. The self energies for $n = 0.83$ to 0.87 show linear- T behavior.

C. Effect of negative t' on QCP

The single-band Hamiltonian used to model the hole-doped cuprates generally includes a negative next-neighbor hopping t' . For such a $t' (< 0)$, the temperature dependence of the self energies with $\omega = 0$ are shown in Fig. 10. We find a wider range of fillings, $n = 0.83$ to 0.87 , to have linear behavior of $\Sigma''(\mathbf{k}_F, \omega = 0)$ shown in Eqn. (10). This scenario is consistent with the phase diagram obtained by Khatami et al.⁶⁶. The inclusion of negative t' deviates the system from the QCP but the

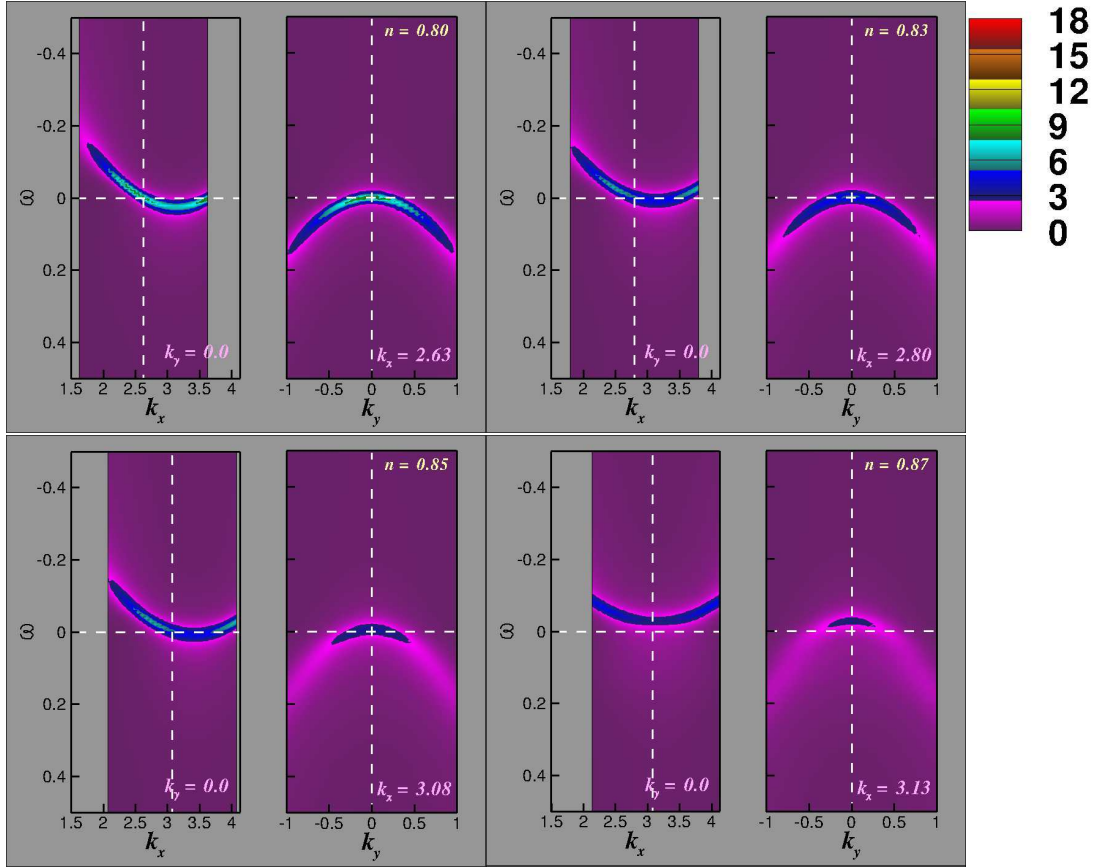


FIG. 11: (color online) Energy dispersion obtained from the peaks of spectral function $A(\mathbf{k}, \omega)$ for various fillings around the Fermi vector k_F along the anti-nodal direction for $t'/t = -0.1$.

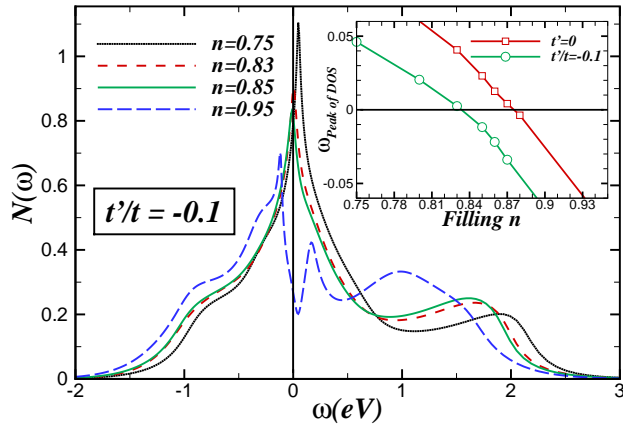


FIG. 12: (Color online) Single-particle density of states for $t'/t = -0.1$ when $U = 6t$, $N_c = 16$, $4t = 1$, and $\beta = 58$. (inset) Comparison of the filling dependence of the position of the peak of the DOS (ω_p) for $t' = 0$ and $t'/t = -0.1$. As the filling changes, ω_p for $t' = 0$ crosses the Fermi level more quickly than that for $t'/t = -0.1$.

effect of the QCP is observed in a larger range of doping (also see Fig. 17).

The inclusion of a t' (< 0) in the Hubbard model results in the pinning of the van Hove singularity to the Fermi level for a larger range of fillings (0.83-0.86) as shown in Fig. 11. If we take the viewpoint that the quantum critical point and pinning of the van Hove singularity to the Fermi level are concomitant, then negative t' leads a range of fillings to be quantum critical and we will see the signatures of this behavior in various transport properties discussed in section III D. Thus both the pictures derived from the temperature dependence of the self-energy and the pinning of the van Hove singularity to the Fermi level are consistent.

Fig. 12 shows density of states for $t'/t = -0.1$ for various fillings as a function of ω . For a given filling, the inset of Fig. 12 shows that the peak in the density of states for $t' < 0$ is slightly shifted to the small frequency in comparison with the peak in the DOS for $t' = 0$. The peak with a low- ω particle-hole symmetry is roughly at $n = 0.84$, not $n = 0.88$ as for $t' = 0$. Moreover, if we use $\Delta\omega_p/\Delta n$, where ω_p is the location of peak in DOS and n is the filling, to estimate the rate at which the peak crosses the Fermi level ($\omega = 0$), we find that the peak of DOS for $t' = 0$ crosses the Fermi level more quickly

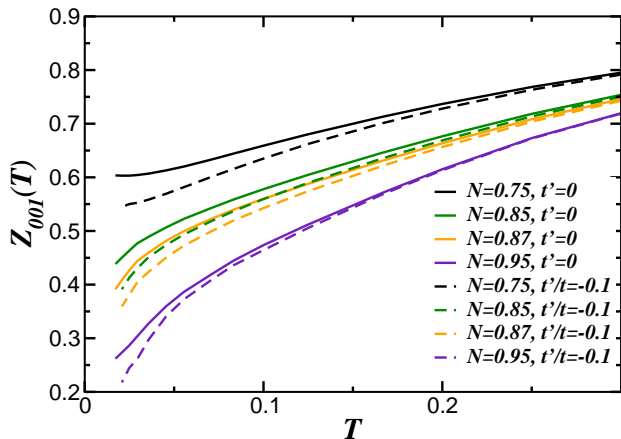


FIG. 13: (Color online) Temperature dependence of the Matsubara fraction Z_0 along the anti-nodal direction for various fillings and with negative next-near-neighbor hopping t' . At the same filling and the same temperature, the Matsubara fraction decreases when $t' < 0$.

than that for negative t' . This can be seen in the inset of Fig. 12 that shows the filling dependence of the location of peak in DOS. This dependence has a steeper slope for $t' = 0$ than that for $t'/t = -0.1$ at the Fermi level. This also implies that negative t' leads to a *wider* range of fillings to have quantum critical properties.

Another interesting point to be noted here is that, when compared to the $t' = 0$ result, the quasi-particle peaks become more incoherent (decreasing Matsubara Z^{53} in Fig. 13) as the filling is increased. This can be seen through the increase of blue color in the dispersion curve in Fig. 11 as the filling is increased.

D. Transport Properties

It is difficult to detect the presence of the van Hove singularity in the dispersion by direct probes like Angle resolved photoemission spectroscopy (ARPES). So we revert to studies of transport properties that provide an indirect method of validating the van Hove singularity picture.

Using the Kubo formula under the relaxation time approximation in Eqn. (11) and Eqn. (12), we obtain the transport properties such as resistivity, thermal conductivity, and thermopower in the Fermi liquid, marginal Fermi liquid, and pseudo-gap regions. Linear resistivity reveals evidence of the marginal Fermi liquid because the electronic cross section is proportional to $-\Sigma''(\mathbf{k}_F, \omega = 0)$ at low T , as seen in Fig. 4 and Fig. 10. Fig. 14 shows the resistivity as a function of temperature for $t' = 0$ and $t'/t = -0.1$ respectively. Again, a narrow range of fillings ($n = 0.85$ and 0.86) for $t' = 0$ allows resistivity proportional to T at low T , while a larger range of fillings ($n = 0.83$ to 0.87) for $t'/t = -0.1$ exhibits linear- T resistivity. The linear resistivity in the marginal Fermi

liquid region is consistent with experiments.^{37–40} We will further discuss the scenario of the phase diagram near the QCP in section IV. For $n = 0.75$, both $t' = 0$ and $t'/t = -0.1$ show the Fermi liquid character—the resistivity goes to zero quadratically when T goes to zero.

According to the the Wiedemann-Franz Law, $\kappa/(\sigma T) = \pi^2/3$ ($k_B = e = 1$), the thermal conductivity of a Fermi liquid is inversely proportional to T .⁵⁰ Fig. 15 shows that $\kappa \propto 1/T$ for $n = 0.75$ when $t' \leq 0$. The inset shows that, for $n = 0.75$, the Wiedemann-Franz ratio $\kappa/(\sigma T)$ approaches a constant which is less than $\pi^2/3$ when $T \leq 0.08$. Dahm et al.⁶⁷ investigated the two-dimensional Hubbard model for $n \simeq 0.9$ and found the smaller Wiedemann-Franz ratio. However, we find that the Wiedemann-Franz ratio is larger than $\pi^2/3$ for the marginal Fermi liquid ($n = 0.85$) and pseudo-gap ($n = 0.95$) regions. We also see that the thermal conductivity becomes very small as $T \rightarrow 0$ for $n = 0.95$ and saturates to a constant for $n = 0.85$ in Fig. 15. So the marginal Fermi liquid seems to separate the property of κ between the Fermi liquid and pseudo-gap. The dashed curves in the Fig. 15 refer to the case $t'/t = -0.1$, and are always below the solid curves for κ but above the solid curves for the ratio κ/σ . This implies that the negative t' reduces the thermal conductivity more than the electrical conductivity.

The thermopower is defined in Eqn. (13). Chakraborty et al.⁵¹ argue that the QCP filling corresponds to the zero-crossing of the thermopower when plotted versus T , indicating that the low-energy particle-hole symmetry is generated. Also in the Fermi liquid theory,⁶⁴ if we assume the relaxation time and electron group velocity are constants, the thermopower is proportional to the derivative of the logarithm of the DOS at the Fermi level. However, the square of single-particle spectra in Eqn. (12) is approximated by $\delta(\omega)\tau_{\mathbf{k}}$ where $\tau_{\mathbf{k}}$ is the relaxation time with a \mathbf{k} -dependence. In addition, the electron group velocity we used here also has a \mathbf{k} -dependence:

$$v^x(\mathbf{k}) = \frac{\partial \epsilon_{\mathbf{k}}^0}{\partial k_x} = 2t \sin k_x + 4t' \sin k_x \cos k_y. \quad (17)$$

If we compare the Kubo $\mathcal{D}_{xx}(\omega)$ (the inset of Fig. 16) and DOS (Fig. 5) in different fillings, we find that the effect of $(v^x(\mathbf{k}))^2$ pulls the peaks of DOS to the left, because the modulation of the $\sin k_x$ suppresses the contribution of the van Hove singularity at $X(\pi, 0)$ and contributes more energies below the Fermi level ($\omega < 0$). As a result, the zero-crossing of thermopower (zero slope of $\mathcal{D}(\omega)$) cannot completely reflect the particle-hole symmetry of DOS ($n = 0.88$ for $t' = 0$). Fig. 16 shows the thermopower S as a function of fillings. For $t' = 0$ and $\beta = 58$, the filling at which S across zero is roughly 0.84 . We expect that zero-crossing of thermopower would approach the critical filling (0.85) when $T \rightarrow 0$.

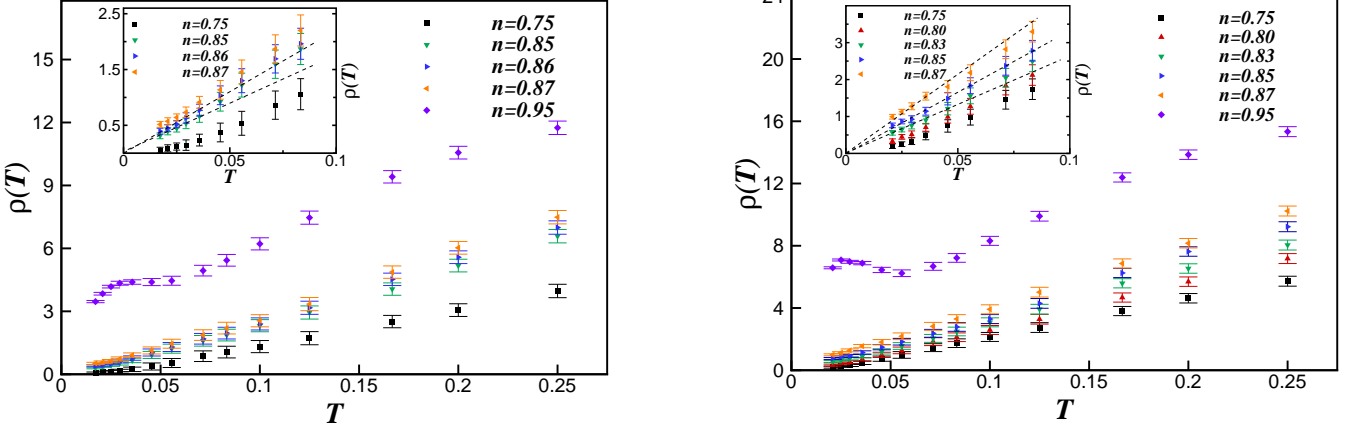


FIG. 14: (Color online) Resistivity versus temperature for (left) $t' = 0$ and (right) $t'/t = -0.1$ with $U = 6t$, $N_c = 16$, and $4t = 1$. The dashed lines in the inset are linear fits. For $t' = 0$, the resistivity shows linear- T behavior for $n = 0.85$ to $n = 0.86$. For $t'/t = -0.1$, the resistivity shows linear- T behavior for $n = 0.83$ to $n = 0.87$.

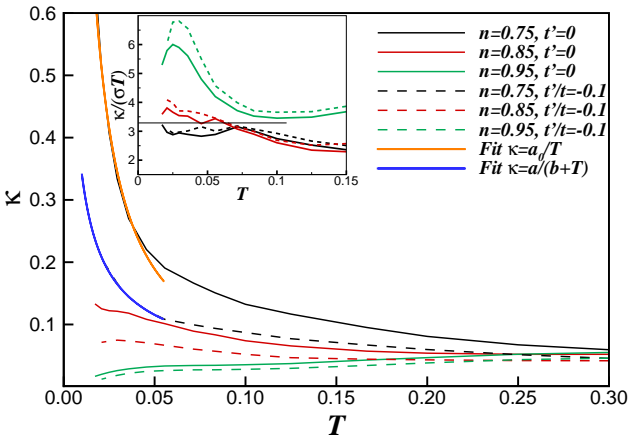


FIG. 15: (Color online) Thermal conductivity versus temperature for $U = 6t$, $N_c = 16$, and $4t = 1$. (inset) Wiedemann Franz ratio for the same physical parameters. The horizontal solid line labels the constant $\pi^2/3$.

IV. DISCUSSION

In our present work, we focus on the role of the van Hove singularity near the quantum critical point (QCP) in the Hubbard model. Near the QCP, we find that the van Hove singularity is pinned to the Fermi level (Fig. 6) and the low energy DOS exhibits particle-hole symmetry (Fig. 5). It is a well-known fact within DMFT¹⁵ that if the van Hove singularity is pinned to the Fermi level for the non-interacting case, it remains pinned even for the interacting case due to momentum independent self-energy. This happens at half-filling for $t' = 0$. The new result of our DCA work is that this pinning of the van Hove singularity to the Fermi level occurs away from half

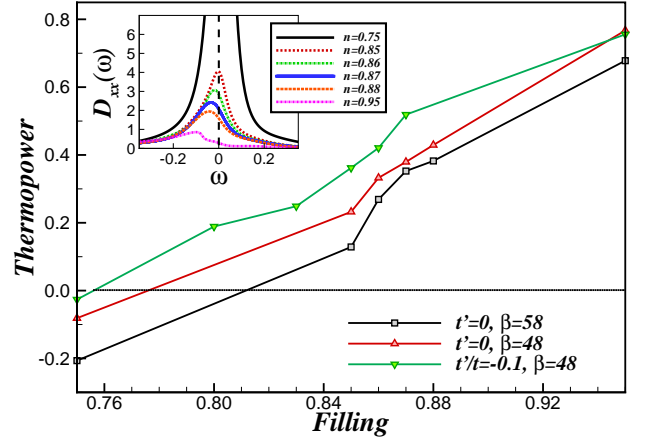


FIG. 16: (Color online) Thermopower as a function of fillings for $U = 6t$, $N_c = 16$, and $4t = 1$ (Lines are guides to the eyes). (inset) Frequency dependence of $D_{xx}(\omega)$ (c.f. Eqn. (12)) for different fillings when $\beta = 58$. The slope of $D_{xx}(\omega)$ at $\omega = 0$ is proportional to the thermopower according to the Eqn. (13).

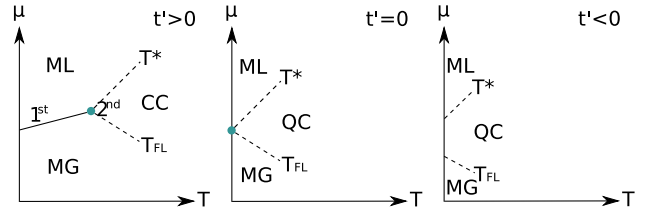


FIG. 17: Schematic $\mu - T$ phase diagram for three values of t' : (left) $t' > 0$, (center) $t' = 0$, and (right) $t' < 0$. CC (QC) means classical (quantum) criticality. ML (MG) means Mott liquid (gas).

filling for $t' = 0$.

In a recent work,⁵⁴ the bare d-wave pairing susceptibility (χ'_{0d}) was found to decay algebraically as $\frac{1}{\sqrt{T}}$ and not logarithmically at the QCP giving rise to a higher T_c . The role of the van Hove singularity pinning in this algebraic quantum critical behavior is explored and it is found that a simple non-interacting picture with a van Hove singularity at the Fermi level does not explain the observed behavior. The standard quadratic dispersion gives logarithmic decay of χ'_{0d} for the half filled model due to the van Hove singularity. As the dispersion is flatter than quadratic near $(\pi, 0)$ (Figs.6, 7), a hypothetical quartic dispersion is considered. It shows the observed algebraic decay for χ'_{0d} but does not give the correct scaling for the imaginary part of the bare susceptibility found in Yang et al.⁵⁴. This can be understood by the vanishing of the spectral weight near the QCP. It means that the singularity in the DOS near the QCP is composed mainly of the incoherent part of the spectral function. Thus the non-interacting picture of the van Hove singularity at the Fermi level does not *completely* describe the critical temperature dependence of the bare susceptibility.

Next we have considered the effect of next-neighbor hopping $t' < 0$ on the single particle dispersion. We found that for $t'/t = -0.1$, the van Hove singularity remains in close proximity of the Fermi level for a range of fillings ($0.83 \leq n \leq 0.86$). As the van Hove singularity “pinning” is attributed to give rise to the marginal Fermi liquid behavior¹¹⁻¹³, we would expect to observe the marginal Fermi liquid behavior for a larger range of fillings. This is confirmed by the linear- T resistivity which is also observed for a wider filling range.

It is hard to detect the presence of the van Hove singularity in photoemission experiments due to matrix element effect.^{68,69} That’s why the indirect probes like transport measurements become crucially important. We have considered the transport properties near the quantum critical point next.

We explore the single particle self energy at low T for $t' = 0$. In Fig. 3, we find that the imaginary part of the self energy is quadratic in ω for the Fermi liquid filling, e.g., $n = 0.75$ and linear in ω for the marginal Fermi liquid filling, e.g., $n = 0.85$, agrees with the marginal Fermi liquid theory.⁵² Moreover, both resistivity and self energy $\Sigma''(\mathbf{k}_F, \omega = 0)$ show quadratic dependence on T for the Fermi liquid and linear- T behavior for the marginal Fermi liquid (Figs. 4, 14). The linear- T in resistivity or the marginal Fermi liquid behavior is observed for the same fillings where the van Hove singularity is pinned to the Fermi level, thus providing an indirect evidence for the presence of the van Hove singularity.

In addition, the resistivities for various t' give information about the $\mu - T$ phase diagram shown in Fig. 17. When $t' > 0$, the critical point is a second order critical point at finite temperature.^{66,70} In analogy with the phase diagram of water, the phase above the first order transition line is an incompressible spin liquid and

named as Mott liquid (ML), and the phase below is a weakly compressible Fermi liquid named as Mott gas (MG). When $t' \rightarrow 0$, the critical point goes to zero temperature and thus is a QCP. This point separates the Fermi liquid and pseudo-gap phases. Above the QCP, the marginal Fermi liquid phase is found to exist in the V-shape quantum critical region. Inside this quantum critical region, the only scale in the self energy is the temperature (like Eqns. 9 and 10). T^* is the temperature separating the marginal Fermi liquid and pseudo-gap. T^* does not separate the quantum critical region from a region of hidden order. Rather in our scenario, it is only the boundary of the quantum critical region. As we cross from the quantum critical region to the Mott liquid, the character of the Mott liquid becomes apparent including a pseudo-gap. For the QCP, both T and negative t' are relevant variables, which are roughly isotropic in their effect. Thus when $t' < 0$, the QCP may be viewed as moving to negative temperatures so that the quantum critical region broadens to allow the linear- T resistivity and the proximity of the van Hove singularity to the Fermi level, to exist in a wider range of fillings.

The thermal conductivity κ in Fig. 15 shows $1/T$ behavior for the Fermi liquid, but weakly depends on T for the marginal Fermi liquid and pseudo-gap. The inset of Fig. 15 shows the Wiedemann Franz law holds for the Fermi liquid but is violated for the marginal Fermi liquid and pseudo-gap. However, it’s difficult to see experimental evidence for this behavior at the marginal Fermi liquid and pseudo-gap fillings because the phonon’s contribution always dominates the electronic contribution for κ above $100K$. To support the van Hove singularity scenario, we can see the signature of the thermopower S in fig. 16 that gives us the evidence of low-energy particle-hole symmetry ($S = 0$) at low temperature. However, due to the effect of \mathbf{k} -dependence of the relaxation time and the electron group velocity, the filling at which the thermopower crosses zero does not occur at the filling with the particle-hole symmetry in DOS.

Thus, we conclude that the quantum critical point in the Hubbard model is accompanied by an extended van Hove singularity in the single particle dispersion pinned near the Fermi level. Both T and negative t' are relevant variables for the quantum critical point, and both the transport and the motion of the van Hove singularity with filling suggest that they are roughly isotropic in their effect. In particular, the extent of fillings displaying quantum criticality expands when t' becomes negative. Transport properties also provide indirect evidence for the presence of the van Hove singularity in the single particle dispersion. The proximity of the van Hove singularity to the QCP within the superconducting dome suggests that the van Hove singularity may be responsible for the enhancement of T_c due to the observed algebraic decay of the bare d-wave pairing susceptibility. However, we find that even a non-interacting van Hove singularity with a quartic dispersion does not give the correct scaling for the imaginary part of bare susceptibility found in

Acknowledgments

We would like to thank Piers Coleman, Jan Zaanen, Thomas Pruschke, Ka-Ming Tam and Jian-Huang She for useful conversations. This work is supported by DOE SciDAC DE-FC02-06ER25792 (SP, SY, KM, MJ), NSF

grants OISE-0952300 (KSC, JM) and DMR-0706379 (DG and MJ). Supercomputer support was provided by the NSF TeraGrid under grant number TG-DMR100007. This research also used resources of the National Center for Computational Sciences at Oak Ridge National Laboratory, which is supported by the Office of Science of the U.S. Department of Energy under Contract No. DE-AC05-00OR22725.

-
- ¹ J. Labbè and J. Bok, *Europhys. Lett.* **3**, 1225 (1987).
² J. Friedel, *J. Phys. (Paris)* **48**, 1787 (1987).
³ D. M. Newns, H. R. Krishnamurthy, P. C. Pattnaik, C. C. Tsuei, and C. L. Kane, *Phys. Rev. Lett.* **69**, 1264 (1992).
⁴ R. S. Markiewicz, *J. Phys. Chem. Solids* **58**, 1179 (1997).
⁵ D. S. Dessau, Z.-X. Shen, D. M. King, D. S. Marshall, L. W. Lombardo, P. H. Dickinson, A. G. Loeser, J. DiCarlo, C.-H. Park, A. Kapitulnik, et al., *Phys. Rev. Lett.* **71**, 2781 (1993).
⁶ K. Gofron, J. C. Campuzano, A. A. Abrikosov, M. Lindroos, A. Bansil, H. Ding, D. Koelling, and B. Dabrowski, *Phys. Rev. Lett.* **73**, 3302 (1994).
⁷ A. Abrikosov, J. Campuzano, and K. Gofron, *Physica C: Superconductivity* **214**, 73 (1993).
⁸ J. C. Campuzano, K. Gofron, H. Ding, R. Liu, B. Dabrowski, and B. J. W. Veal, *J. Low Temp. Phys.* **95**, 245 (1994).
⁹ D. M. King, Z. X. Shen, D. S. Dessau, D. S. Marshall, C. H. Park, W. E. Spicer, J. L. Peng, Z. Y. Li, and R. L. Greene, *Phys. Rev. Lett.* **73**, 3298 (1994).
¹⁰ A. Piriou, N. Jenkins, C. Berthod, I. Maggio-Aprile, and O. Fischer, *Nat. Commun.* **2**, 221 (2011).
¹¹ P. C. Pattnaik, C. L. Kane, D. M. Newns, and C. C. Tsuei, *Phys. Rev. B* **45**, 5714 (1992).
¹² D. M. Newns, C. C. Tsuei, R. P. Huebener, P. J. M. van Bentum, P. C. Pattnaik, and C. C. Chi, *Phys. Rev. Lett.* **73**, 1695 (1994).
¹³ C. C. Tsuei, D. M. Newns, C. C. Chi, and P. C. Pattnaik, *Phys. Rev. Lett.* **65**, 2724 (1990).
¹⁴ C. M. Varma, P. B. Littlewood, S. Schmitt-Rink, E. Abrahams, and A. E. Ruckenstein, *Phys. Rev. Lett.* **63**, 1996 (1989).
¹⁵ P. Majumdar and H. R. Krishnamurthy, *cond-mat/9604057v1* (1996).
¹⁶ F. Assaad and M. Imada, *Eur. Phys. J. B* **10**, 595 (1999).
¹⁷ M. Imada, A. Fujimori, and Y. Tokura, *Rev. Mod. Phys.* **70**, 1039 (1998).
¹⁸ E. Dagotto, A. Nazarenko, and M. Boninsegni, *Phys. Rev. Lett.* **73**, 728 (1994).
¹⁹ J. L. McChesney, A. Bostwick, T. Ohta, T. Seyller, K. Horn, J. González, and E. Rotenberg, *Phys. Rev. Lett.* **104**, 136803 (2010).
²⁰ D. M. Newns, P. C. Pattnaik, and C. C. Tsuei, *Phys. Rev. B* **43**, 3075 (1991).
²¹ S. Gopalan, O. Gunnarsson, and O. K. Andersen, *Phys. Rev. B* **46**, 11798 (1992).
²² D. M. Newns, C. C. Tsuei, and P. C. Pattnaik, *Phys. Rev. B* **52**, 13611 (1995).
²³ I. Dzyaloshinskii, *J. Phys. I France* **6**, 119 (1996).
²⁴ D. Djajaputra and J. Ruvalds, *cond-mat/9604057v1* (1996).
²⁵ R. G. Dias, *J. Phys.: Condens. Matt.* **12**, 9053 (2000).
²⁶ C. J. Halboth and W. Metzner, *Phys. Rev. B* **61**, 7364 (2000).
²⁷ G. Kastinakis, *Physica C: Superconductivity* **340**, 119 (2000).
²⁸ V. Y. Irkhin and A. A. Katanin, *Phys. Rev. B* **64**, 205105 (2001).
²⁹ V. Y. Irkhin, A. A. Katanin, and M. I. Katsnelson, *Phys. Rev. Lett.* **89**, 076401 (2002).
³⁰ A. A. Katanin and A. P. Kampf, *Phys. Rev. Lett.* **93**, 106406 (2004).
³¹ K. M. Shen, N. Kikugawa, C. Bergemann, L. Balicas, F. Baumberger, W. Meevasana, N. J. C. Ingle, Y. Maeno, Z.-X. Shen, and A. P. Mackenzie, *Phys. Rev. Lett.* **99**, 187001 (2007).
³² T. Shibauchi, L. Krusin-Elbaum, M. Hasegawa, Y. Kasahara, R. Okazaki, and Y. Matsuda, *Proc. Natl. Acad. Sci. U.S.A.* **105**, 7120 (2008).
³³ A. Tamai, M. P. Allan, J. F. Mercure, W. Meevasana, R. Dunkel, D. H. Lu, R. S. Perry, A. P. Mackenzie, D. J. Singh, Z.-X. Shen, et al., *Phys. Rev. Lett.* **101**, 026407 (2008).
³⁴ A. Katanin, *Phys. Rev. B* **81**, 165118 (2010).
³⁵ S. E. Sebastian, N. Harrison, M. M. Altarawneh, C. H. Mielke, R. Liang, D. A. Bonn, W. N. Hardy, and G. G. Lonzaricha, *PNAS* **107**, 6175 (2010).
³⁶ L. Taillefer, *Annu. Rev. Condens. Matter Phys.* **1**, 51 (2010).
³⁷ Y. Ando, S. Komiya, K. Segawa, S. Ono, and Y. Kurita, *Phys. Rev. Lett.* **93**, 267001 (2004).
³⁸ R. Daou, N. Doiron-Leyraud, D. LeBoeuf, S. Y. Li, F. Laliberte, O. Cyr-Choiniere, Y. J. Jo, L. Balicas, J.-Q. Yan, J.-S. Zhou, et al., *Nat. Phys.* **5**, 31 (2009).
³⁹ R. A. Cooper, Y. Wang, B. Vignolle, O. J. Lipscombe, S. M. Hayden, Y. Tanabe, T. Adachi, Y. Koike, M. Nohara, H. Takagi, et al., *Science* **323**, 603 (2009).
⁴⁰ M. Gurvitch and A. T. Fiory, *Phys. Rev. Lett.* **59**, 1337 (1987).
⁴¹ B. Wuyts, V. V. Moshchalkov, and Y. Bruynseraede, *Phys. Rev. B* **53**, 9418 (1996).
⁴² C. Uher, A. B. Kaiser, E. Gmelin, and L. Walz, *Phys. Rev. B* **36**, 5676 (1987).
⁴³ A. J. Schofield, *Contemporary Physics* **40**, 95 (1999).
⁴⁴ X. F. Sun, S. Komiya, and Y. Ando, *Phys. Rev. B* **67**, 184512 (2003).
⁴⁵ R. K. Williams, J. O. Scarbrough, J. M. Schmitz, and J. R. Thompson, *Phys. Rev. B* **57**, 10923 (1998).

- ⁴⁶ S. Chakraborty, D. Galanakis, and P. Phillips, arXiv:0807.2854v2.
- ⁴⁷ H. J. Trodahl, Phys. Rev. B **51**, 6175 (1995).
- ⁴⁸ M. Gurvitch, J. M. Valles, A. M. Cucolo, R. C. Dynes, J. P. Garno, L. F. Schneemeyer, and J. V. Waszczak, Phys. Rev. Lett. **63**, 1008 (1989).
- ⁴⁹ F. Steglich, *High temperature superconductors and materials and mechanisms of superconductivity* (North Holland, Amsterdam, 1988), p. 1010.
- ⁵⁰ G. Wiedemann and R. Franz, Ann. Phys. **89**, 497 (1853).
- ⁵¹ S. Chakraborty, D. Galanakis, and P. Phillips, Phys. Rev. B **82**, 214503 (2010).
- ⁵² C. M. Varma, Z. Nussinov, and W. van Saarloos, Phys. Rep. **361**, 267 (2002).
- ⁵³ N. S. Vidhyadhiraja, A. Macridin, C. Sen, M. Jarrell, and M. Ma, Phys. Rev. Lett. **102**, 206407 (2009).
- ⁵⁴ S.-X. Yang, H. Fotsos, S.-Q. Su, D. Galanakis, E. Khatami, J.-H. She, J. Moreno, J. Zaanen, and M. Jarrell, Phys. Rev. Lett. **106**, 047004 (2011).
- ⁵⁵ M. Jarrell and J. E. Gubernatis, Physics Reports **269**, 133 (1996).
- ⁵⁶ X. Wang, E. Gull, L. de' Medici, M. Capone, and A. J. Millis, Phys. Rev. B **80**, 045101 (2009).
- ⁵⁷ M. H. Hettler, A. N. Tahvildar-Zadeh, M. Jarrell, T. Pruschke, and H. R. Krishnamurthy, Phys. Rev. B **58**, R7475 (1998).
- ⁵⁸ M. H. Hettler, M. Mukherjee, M. Jarrell, and H. R. Krishnamurthy, Phys. Rev. B **61**, 12739 (2000).
- ⁵⁹ J. E. Hirsch and R. M. Fye, Phys. Rev. Lett. **56**, 2521 (1986).
- ⁶⁰ M. Jarrell, T. Maier, C. Huscroft, and S. Moukouri, Phys. Rev. B **64**, 195130 (2001).
- ⁶¹ A. N. Rubtsov, V. V. Savkin, and A. I. Lichtenstein, Phys. Rev. B **72**, 035122 (2005).
- ⁶² N. Blümer, Phys. Rev. B **76**, 205120 (2007).
- ⁶³ R. Kubo, *Lectures in Theoretical Physics* (New York, Interscience, 1959), vol. 1, p. 120.
- ⁶⁴ J. A. Sto/vneng and P. Lipavský, Phys. Rev. B **42**, 9214 (1990).
- ⁶⁵ A. C. Hewson, *The Kondo Problem to Heavy Fermions* (Cambridge University Press, Cambridge, 1993).
- ⁶⁶ E. Khatami, K. Mielson, D. Galanakis, A. Macridin, J. Moreno, R. T. Scalettar, and M. Jarrell, Phys. Rev. B **81**, 201101 (2010).
- ⁶⁷ T. Dahm, L. Tewordt, and S. Wernbter, Phys. Rev. B **49**, 748 (1994).
- ⁶⁸ A. Bansil and M. Lindroos, J. Phys. Chem. Solids **59**, 1879 (1998).
- ⁶⁹ A. Bansil and M. Lindroos, Phys. Rev. Lett. **83**, 5154 (1999).
- ⁷⁰ A. Macridin, M. Jarrell, and T. Maier, Phys. Rev. B **74**, 085104 (2006).

